ORIGINAL ARTICLE

Deformation mechanism analysis of three-roller continuous and synchronous calibration process of straightness and roundness for LSAW pipes

Xueying Huang[1] · Gaochao Yu[2,4] · Chunge Wang[3] · Jun Zhao[2]

Abstract

The continuous and synchronous calibration process for straightness and roundness of LSAW (longitudinally submerged arc welding, LSAW) pipes with three rollers is a bidirectional reciprocating bending process. It includes both axial and circumferential directions. It is particularly important to reveal the deformation mechanism, which provides theoretical support for the calibration process to be applied to actual production. Based on this, through the combination of references, theoretical analysis and numerical simulation, the deformation mechanism is analyzed in this paper. The whole deformation process of pipe is modeled and then numerically simulated with FEM software of ABAQUS. The results show that reciprocating bending can eliminate the difference of initial curvature, so that the axial curvature and circumferential curvature are unified to the same direction and value, respectively. The calibration process of LSAW pipes is realized by the synergy between the axial reciprocating bending straightening process and the circumferential reciprocating bending rounding process. The simulation and experimental results support the theoretical results, and the deformation is mainly caused by axial stress and circumferential stress.

Keywords LSAW pipes · Three-roller · Continuous and synchronous calibration process · Deformation mechanism · Numerical simulations · Axial and circumferential bidirectional reciprocating bending

Highlights
- Through the combination of references, theoretical analysis and numerical simulation, the deformation mechanism of the calibration process has been analyzed.
- The deformation mechanism analysis provides theoretical guidance for the application of the process to actual production.
- The analysis method provides a new idea for simplifying the problem of three-dimensional deformation.

✉ Gaochao Yu
gch_yu@ysu.edu.cn

Xueying Huang
huangxueying@nbufe.edu.cn

Chunge Wang
wangchunge@nbt.edu.cn

Jun Zhao
zhaojun@ysu.edu.cn

1   School of Digital Technology and Engineering, Ningbo University of Finance and Economics, Ningbo City 315175, People's Republic of China

2   Key Laboratory of Advanced Forging & Stamping Technology and Science (Yanshan University), Ministry of Education of China, Qinhuangdao City 066004, People's Republic of China

3   School of Mechanical and Energy Engineering, NingboTech University, Ningbo City 315100, People's Republic of China

4   College of Mechanical Engineering, Yanshan University, No.438, Hebei Street, Haigang District, P.O.Box 066004, Qinhuangdao, People's Republic of China

1 Introduction

With the development of the world's oil and gas resources transferring to unconventionality, remote and harsh development environment and the development trend of oversized transmission have put forward higher requirements for pipeline construction. Longitudinally submerged arc welding (LSAW) pipes are made from high-steel wide plates, especially for long-distance oil and gas pipeline transportation

and for laying pipes in deep-sea or cold areas. The straightness and roundness of formed welding pipe cannot meet the industrial standards due to the factors such as welding thermal stress, material properties and technical equipment [1–3]. The formed welding pipe needs to be straightened and rounded (the process of straightening and rounding is referred to as the calibration process in this paper). According to the American Petroleum Institute's industry standard ANSI/API Spec. 5L, the straightness and roundness of finished welding pipes have been strictly required. Namely the roundness does not exceed $\pm 0.75\%$ of a nominal outer diameter, and the straightness is not greater than 0.2% of a total length [4].

At present, the roundness calibration process mainly includes the whole-diameter roundness calibration process [5, 6], the over-bending roundness calibration process [7–9] and the roll-type roundness calibration process [10, 11]. Common straightness calibration techniques include the pressure straightening [12–14] and the cross-roll straightening [15–18]. The existing roundness and straightness calibration processes are done separately. On the one hand, it leads to the growth of production process and the reduction of production efficiency, which is not easy to realize automatic and intelligent production; On the other hand, because the deformation process affects each other, the flattening problem of LSAW pipes cannot be solved [19]. It is difficult to adjust both the straightness and roundness to optimal levels, which also seriously affects on-site welding and pipeline safety [20]. In view of the application trend of LSAW pipes and the existing problem of calibration technology, a new three-roller continuous and synchronous calibration process of straightness and roundness was proposed [20–23]. The study of process deformation mechanism provides theoretical support for understanding the essence of the process and applying it to actual production.

Based on the combination of reference, theoretical analysis and numerical simulation, this paper further studies the deformation mechanism of the calibration process. It includes the axial reciprocating bending straightening process and the circumferential reciprocating bending rounding process. In addition, the distribution of equivalent stress, maximum and minimum principal stress of pipe in Section III is analyzed; the effects of axial stress, circumferential stress and radial stress on pipe deformation are discussed. The simulation and experimental results can support the theoretical analysis results.

2 Process introduction

The three-roller continuous and synchronous calibration process of straightness and roundness for LSAW pipes is shown in Fig. 1. The process' main working parts are three parallel rollers, including a convex roller (upper roller) and two concave rollers (lower rollers). Before experiment, each roller pushes the same radial reduction toward the pipe's central axis. During the experiment, two concave rollers rotate simultaneously driven by servo motors. This makes the pipe and convex roller rotate under the action of friction. At the same time, the servo motor drives the push plate to make the pipe move along the slideway, thus finishing the calibration process.

The schematic diagram of roller-shape is shown in Fig. 2. As shown in Fig. 2, both ends of the roller are loading section (Section I) and unloading section (Section V), both of which are truncated cone shape. The design enables the pipe to enter smoothly between the three rollers and ensures that the pipe can unload smoothly, so as to unify the curvature. Sections II and IV are roundness calibration sections, which are cylindrical in shape. The design can make the pipe undergo multiple reciprocating bending along the circumferential direction, resulting in elastic–plastic deformation. Thus, roundness calibration and complementary roundness calibration are realized. Section III is roundness and straightness calibration section. The upper roller part is convex, and the lower roller part is concave. The design ensures that the pipe can undergo multiple reciprocating bending along the circumferential and axial directions. Thereby, roundness and straightness calibration are realized.

The curvature distribution of Section III is shown in Fig. 3. Section III is composed of n tangent arcs with changing

Fig. 1 Schematic diagram of the calibration process
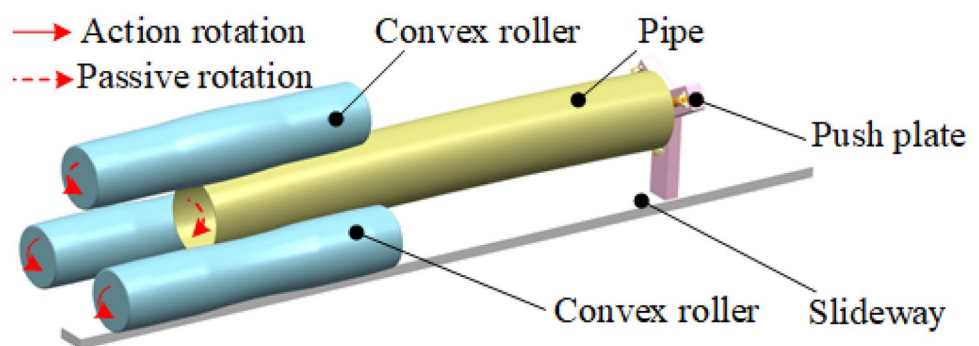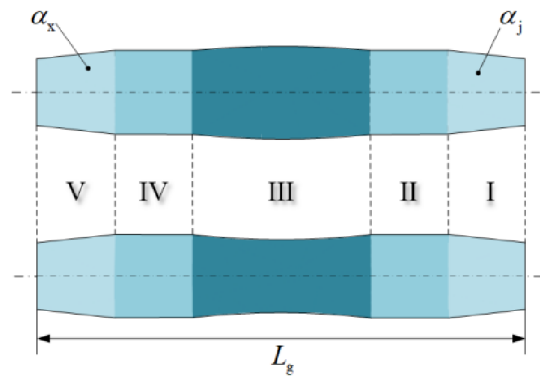
Section I: Loading section; Section II: Roundness calibration section, Section III: Roundness and

straightness calibration section, Section IV: Roundness complement calibration section;

Section V: Unloading section

Fig. 2 Schematic diagram of roller-shape

curvature, whose curvature is gradually reduced from the middle to both ends. That is, K_1 to K_n gradually increases in value, and K_n is the maximum curvature of Section III.

Figure 4 is a schematic diagram of the loading parameter. Three rollers load the same radial reduction toward the pipe center, and the stroke of each roller is recorded as H.

$$H = R_1 + R - H_j \tag{1}$$

where H is the radial reduction, R_1 is the roller radius, R is the pipe radius, and H_j is the distance from the pipe's center to the center of roller after loading.

3 Process deformation mechanism

In this paper, the axial and circumferential reciprocating bending deformation are simplified to the pure bending problem of plane curved beam [24].

3.1 Reciprocating bending springback analysis of axial straightening

The straightening process of the calibration process is an axial reciprocating bending process. As shown in Fig. 3, the
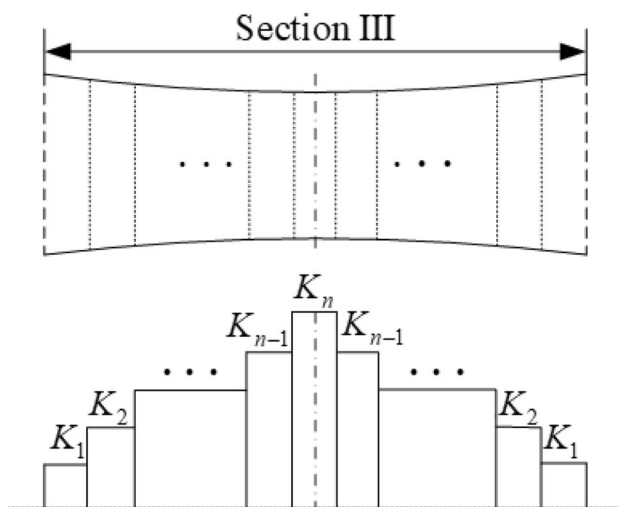

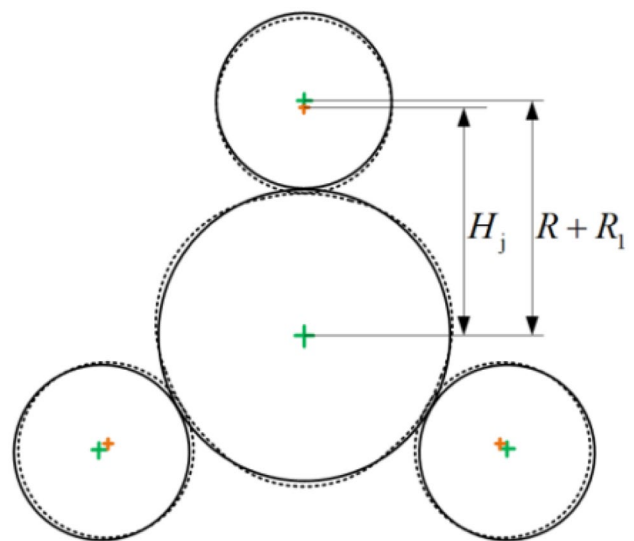**Fig. 3** Curvature distribution of Section III–n-segment curvature

Fig. 4 Diagram of loading parameters

curvature distribution of Section III is constantly changing, with the curvature increasing from zero (K_1) to K_n and then reduced to zero. According to the geometric characteristics of LSAW pipe, a linear simple kinematic hardening (LSKH) constitutive model is adopted [15], as shown in Fig. 5.

The expression is as follows:

$$\sigma = \begin{cases} D\varepsilon + \sigma_0 & \varepsilon > 0 \\ D\varepsilon - \sigma_0 & \varepsilon < 0 \end{cases} \tag{2}$$

$$\sigma_0 = \left(1 - \frac{D}{E}\right)\sigma_s$$

where σ_s is yield stress, D is plastic modulus, and E is elastic modulus.

The circular section of pipe is shown in Fig. 6. The coordinate system is established with the geometric center of the section as the coordinate origin. The bending moment M during loading can be simply described as

$$M = \int_A \sigma z \mathrm{d}z = \begin{cases} DI(K - K_0) + M_0 & K \geq K_0 \\ DI(K - K_0) - M_0 & K < K_0 \end{cases} \tag{3}$$

where $M_0 = \frac{4\sigma_0}{3}(R_1^3 - R_2^3)$, $I = \frac{\pi}{4}(R_1^4 - R_2^4)$, R_2 is the inner diameter of pipe.

Since the deformation of each section is continuous, the current initial curvature can be used as the curvature after the last bending springback. According to Eq. (3), the recurrence equation of reciprocating bending can be expressed as

$$K_{pn} = \begin{cases} K_1 - \frac{M_1(K_1, K_0)}{EI} & n = 1 \\ K_n - \frac{M_n(K_n, K_{p(n-1)})}{EI} & n \geq 2 \end{cases} \tag{4}$$

where n is the times of reciprocating bending and K_{pn} is the springback curvature after reciprocating bending n times.
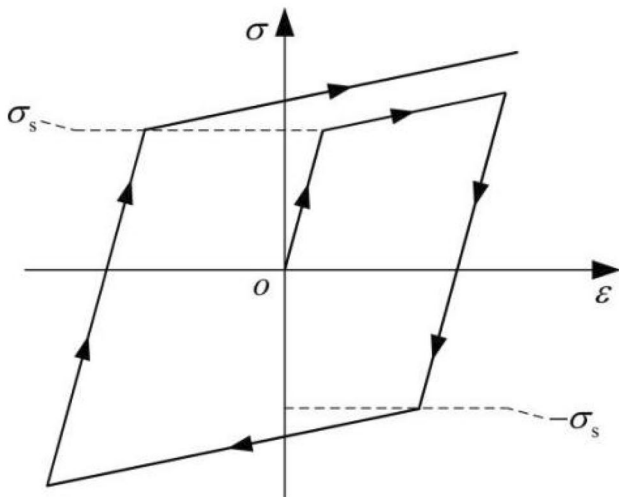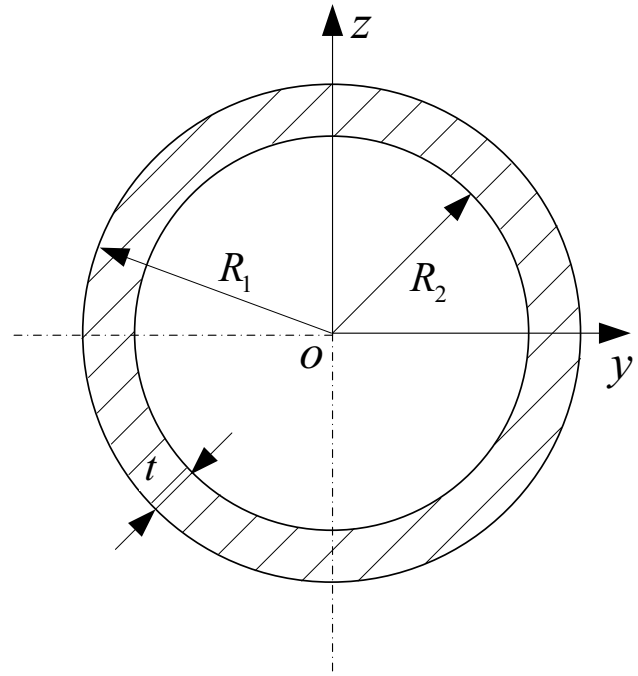

Fig. 5 LSKH constitutive model

Fig. 6 Circular section of pipes

Based on the springback theory of small curvature plane bending [25], the springback curvature of pipe micro-beam after reciprocating bending n times along the axis is deduced by mathematical induction. The reciprocating bending process is shown in Fig. 7.

If the first bending is reverse bending, the unified equation of curvature after springback is

$$K_{pn} = K_n - \frac{D}{E}(K_n - K_{n-1}) - \left(\frac{D}{E}\right)^2(K_{n-1} - K_{n-2}) - \ldots$$
$$- \left(\frac{D}{E}\right)^{n-1}(K_2 - K_1) + (-1)^{n+1}\left(\frac{16\sigma_0(R_1^3 - R_2^3)}{3\pi(R_1^4 - R_2^4)(E + D)}\right) \tag{5}$$

If the first bending is positive bending, the unified equation of curvature after springback is

$$K_{pn} = K_n - \frac{D}{E}(K_n - K_{n-1}) - \left(\frac{D}{E}\right)^2(K_{n-1} - K_{n-2}) - \ldots$$
$$- \left(\frac{D}{E}\right)^{n-1}(K_2 - K_1) + (-1)^n\left(\frac{16\sigma_0(R_1^3 - R_2^3)}{3\pi(R_1^4 - R_2^4)(E + D)}\right) \tag{6}$$

Equations (5) and (6) can be expressed uniformly as

$$\overline{K}_{pn} = f(D, E, \sigma_0, R_1, R_2, K_1, K_2, \ldots, K_n) \tag{7}$$

Equation (7) proves that multiple reciprocating bending can eliminate the difference of initial curvature along the axial direction. This unifies the curvature to the same

Fig. 7 Schematic diagram of reciprocating bending of micro-beam
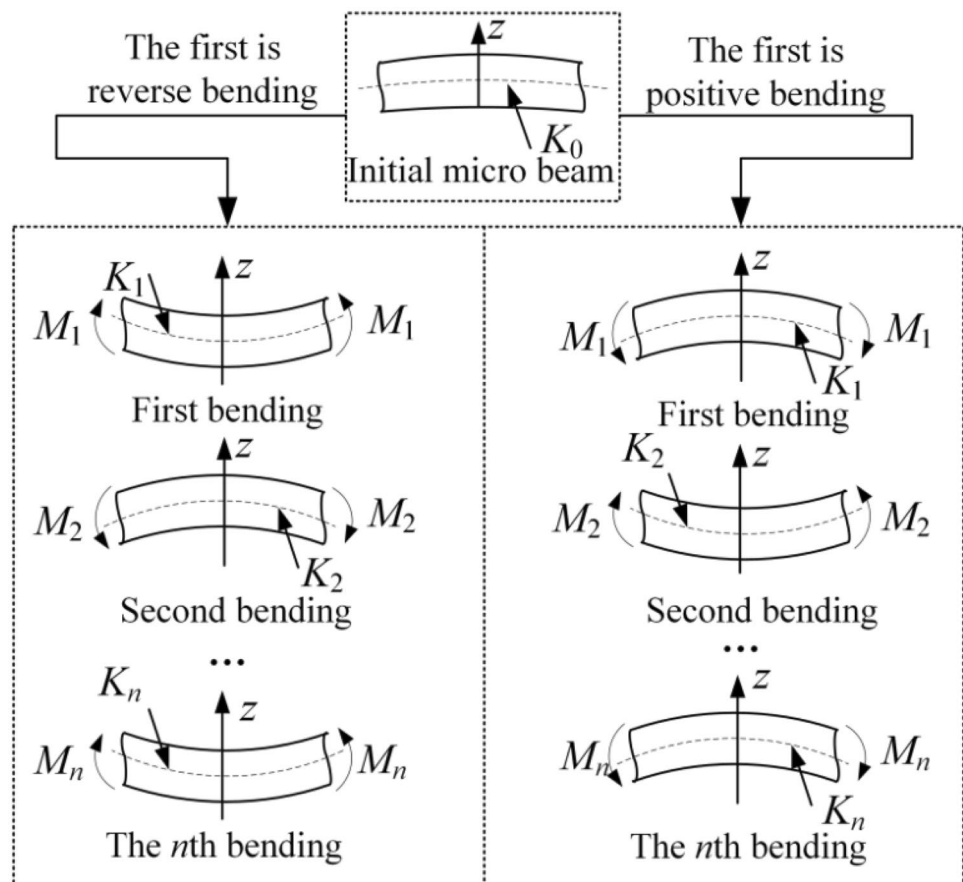
direction and value. $\overline{K}_{pn}$ is related to material properties, inner and outer diameters of pipe and bending curvature. When the loading curvature K_n tends to zero, the springback curvature of the pipe along the axial direction after reciprocating bending is also close to zero, thus achieving straightening.

3.2 Reciprocating bending springback analysis of circumferential rounding

The rounding process of the calibration process is a circumferential reciprocating bending process. Similarly, a linear simple kinematic hardening (LSKH) constitutive model is adopted [15]. The relation between bending moment and curvature can be described as

$$M = \int_A \sigma z \mathrm{d}z = \begin{cases} DI(K - K_0) + M_0 & K \geq K_0 \\ DI(K - K_0) - M_0 & K < K_0 \end{cases} \tag{8}$$

where $M_0 = \frac{\sigma_0 t^2}{4}$.

Then, after reciprocating bending n times, the springback curvature of pipe micro-beam along the circumferential direction is deduced. The reciprocating bending process is shown in Fig. 7. The derivation process is the same as that of axial reciprocating bending.

If the first bending is reverse bending, the unified equation of curvature after springback is

$$K_{pn} = K_n - \frac{D}{E}(K_n - K_{n-1}) - \left(\frac{D}{E}\right)^2 (K_{n-1} - K_{n-2}) - \ldots \\ - \left(\frac{D}{E}\right)^{n-1}(K_2 - K_1) + (-1)^{n+1}\left(\frac{3\sigma_0}{t(E+D)}\right) \tag{9}$$

If the first bending is positive bending, the unified equation of curvature after springback is

$$K_{pn} = K_n - \frac{D}{E}(K_n - K_{n-1}) - \left(\frac{D}{E}\right)^2 (K_{n-1} - K_{n-2}) - \ldots \\ - \left(\frac{D}{E}\right)^{n-1}(K_2 - K_1) + (-1)^{n}\left(\frac{3\sigma_0}{t(E+D)}\right) \tag{10}$$
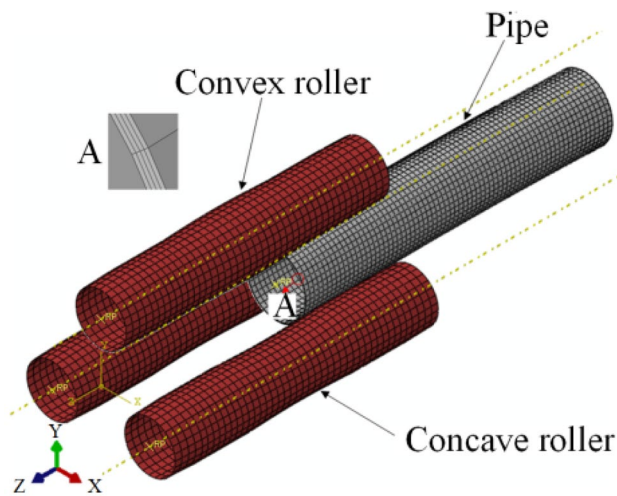
Equations (9) and (10) can be expressed uniformly as

Fig. 8 Finite element model

$$\overline{K}_{pn} = f(D, E, \sigma_0, K_1, K_2, \ldots, K_n) \qquad (11)$$

Equation (11) proves that multiple reciprocating bending can eliminate the difference of initial curvature along the circumferential direction. This unifies the curvature to the same direction and value. $\overline{K}_{pn}$ is related to material properties, thickness of pipe wall and bending curvature. When the loading curvature $\overline{K}_n$ tends to a certain value, the springback curvature of pipe along the circumferential direction after reciprocating bending tends to be consistent, thus achieving rounding.

4 Numerical simulation

Using the software ABAQUS, a finite element model of the LSAW pipe calibration process is established, as shown in Fig. 8. Regardless of the effect of pipe welds on the continuous calibration process, the mechanical properties and geometric dimensions of pipes are shown in Table 1 and the geometric dimensions of rollers are shown in Table 2. The pipe is set as a deformable body. The pipe wall is divided into 4 layers along the thickness, and the pipe is discretized by 8-node linear hexagonal nonconforming

mode elements. Select the continuum distributing coupling method to couple the center point of the pipe cross section and the pipe cross-section boundary, and select all 6 degrees of freedom for the constrained area. The three rollers are set as discrete rigid bodies. The contact between the pipe and each roller is set to pure master–slave contact and motion contact conditions, and the coefficient of friction is 0.2.

5 Results and discussion

During numerical simulation, the roller rotation speed is 150 mm/s and the pipe forward speed is 4 mm/s. The times of reciprocating bending of ST12 pipe from starting to contact the roller to completely separating from the roller is 67.

The equivalent stress distribution of one-half ST12 pipe in Section III is shown in Fig. 9. According to the symmetry, there are three positive bending regions and three reverse bending regions along the circumferential direction. They are evenly distributed in the whole pipe [21].

The distribution of maximum and minimum principal stresses in Section III is shown in Fig. 10. The maximum and minimum principal stress values are shown in Table 3. In combination with Figs. 9 and 10, it can be seen that positions A and C are located in the reverse bending region. The maximum principal stress is generated in the inner layer of the pipe (nodes 97 and 427), and the minimum principal stress is generated in the outer layer of the pipe (nodes 67 and 454). Positions B and D are located in the positive bending region. The maximum principal stress is generated in the outer layer of the pipe (nodes 460 and 448), and the minimum principal stress is generated in the inner layer of the pipe (nodes 421 and 433). Based on the above analysis, the absolute values of the maximum principal stress and the minimum principal stress of the pipe any position are basically equal, which verifies the characteristics of pure bending deformation.

The distribution of axial stress along the thickness and length directions in Section III is shown in Fig. 11. Plastic deformation occurs along the thickness and length directions due to axial stress. It is proved that the geometric

Table 1 Mechanical properties and geometric dimensions of pipes

Material	Elastic modulus E (GPa)	Yield stress σ_s (MPa)	Plastic modulus D (MPa)	Outer diameter D_p (mm)	Length L_p (mm)	Thickness t (mm)	Initial roundness	Initial straightness
ST12	179	189	1500	140	700	2	5%	10‰

Table 2 Geometric dimension of rollers

Outer diameter D_g (mm)	Length L_g (mm)	Proportion of rollers	Taper of Section I (rad)	Taper of Section V (rad)	K_n (mm^{-1})	Roller shape curve of Section III
120	600	1:2:4:2:1	0.033	0.025	0.001	$0.16x^2 - 0.0004y^2 - 1 = 0$

dimension of the longitudinal section of the pipe has changed.

Figure 11a shows the distribution of axial stress along the thickness direction. In the positive bending region, the pipe's outer layer is stretched with a maximum stress of 249 MPa (node 5) and a minimum stress of 0 MPa (node 1); in the reverse bending region, the inner layer of the pipe is compressed with a maximum stress of 0 MPa (node 5) and a minimum stress of -278 MPa (node 1). The above indicates that one part of the pipe wall has reached yield strength, while the other part has produced only elastic deformation.

Figure 11b shows the distribution of axial stress along the length direction. The axial stress of the pipe's outermost nodes increases gradually from both ends to the center along the length direction. And in the center of the roller curve, the axial stress reaches its maximum. That shows that the plastic deformation occurs in Section III along the length direction.

The distribution of tangential stress along the thickness and circumferential directions in Section III is shown in Fig. 12. As indicated in Fig. 12, plastic deformation occurs along the thickness and circumferential directions due to circumferential stress. It is proved that the geometric dimension of the circumferential section of the pipe has changed.
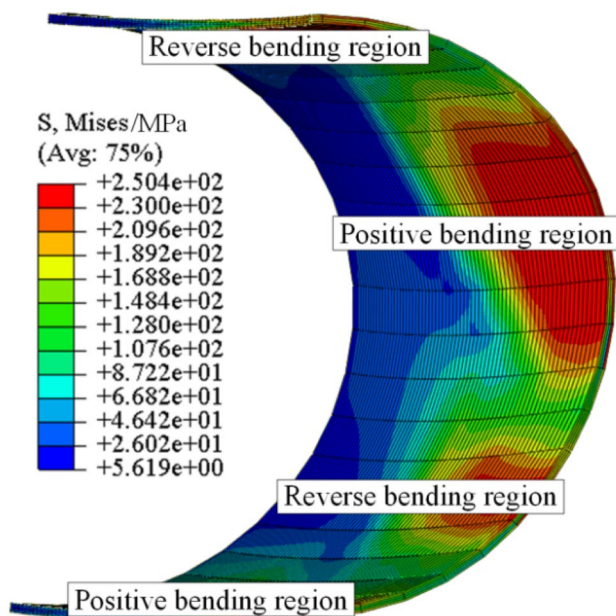
Figure 12a shows the distribution of circumferential stress along the thickness direction. In the positive bending region, the pipe's outer layer is stretched with a maximum stress of 287 MPa (node 5); the inner layer is compressed with a minimum stress of -289 MPa (node 1). In the reverse bending region, the inner layer of the pipe is stretched, the maximum stress is 280 MPa (node 1); the outer layer is compressed, and the minimum stress is -276 MPa (node 5). From this, regardless of the positive bending region or the reverse bending region, the absolute value of the outer and inner circumferential stresses of the pipe is basically the same.

Figure 12b shows the distribution of circumferential stress along the circumferential direction. The circumferential stress values of the pipe's outermost nodes are selected. As can be seen from Fig. 12b, the area of the positive bending region is larger than that of the reverse bending region. This is consistent with the equivalent stress distribution in Fig. 9. The absolute value of circumferential stress reaches the maximum at each region's center and gradually decreases from the center to both ends.

The distribution of radial stress in Section III is shown in Fig. 13. It shows that the radial stress of the pipe is very small, about -2.0 MPa to 2.0 MPa, and only elastic deformation occurs.

The effects of axial, circumferential and radial stresses on the pipe calibration process are discussed through numerical simulation. The results show that the pipe calibration process is realized by the synergy between axial stress and circumferential stress. As a result, the simulation results also support the theoretical analysis results.

The equivalent stress distribution of ST12 pipe after calibration is shown in Fig. 14. It can be observed in Fig. 14 that the distribution of equivalent stress tends to be uniform and the residual stress is small. The simulation results show that the residual roundness is within 0.14% and the residual straightness is within 0.17%. The results meet the standard requirements [4]. As a result, the feasibility of the process is initially verified.
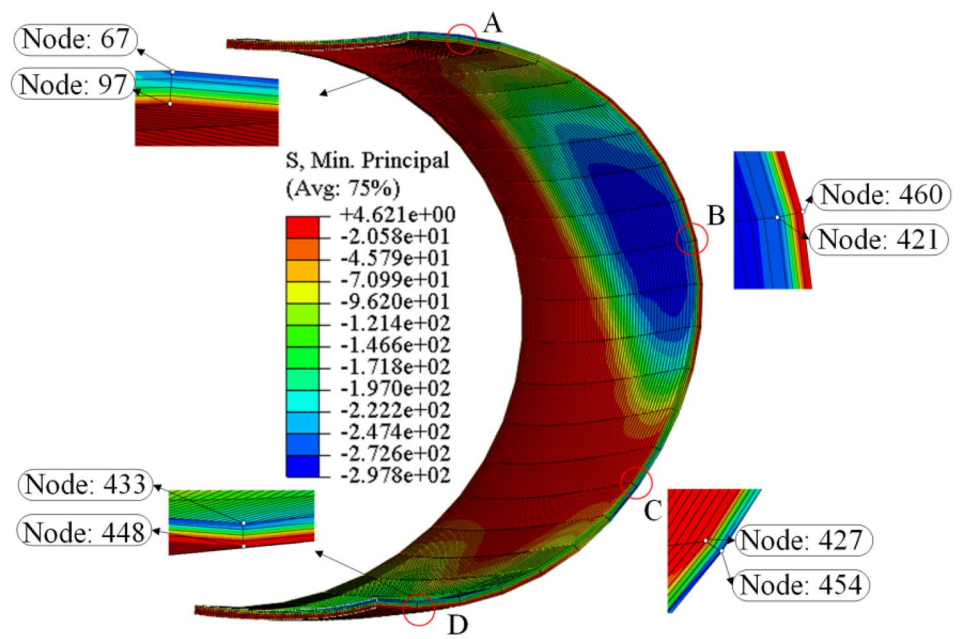
6 Experimental validation

The experimental device for pipe calibration is shown in Fig. 15. The device can realize both continuous rounding and continuous straightening of LSAW pipes.

Fig. 9 Equivalent stress distribution of one-half pipe

Fig. 10 Distribution of maximum and minimum principal stresses
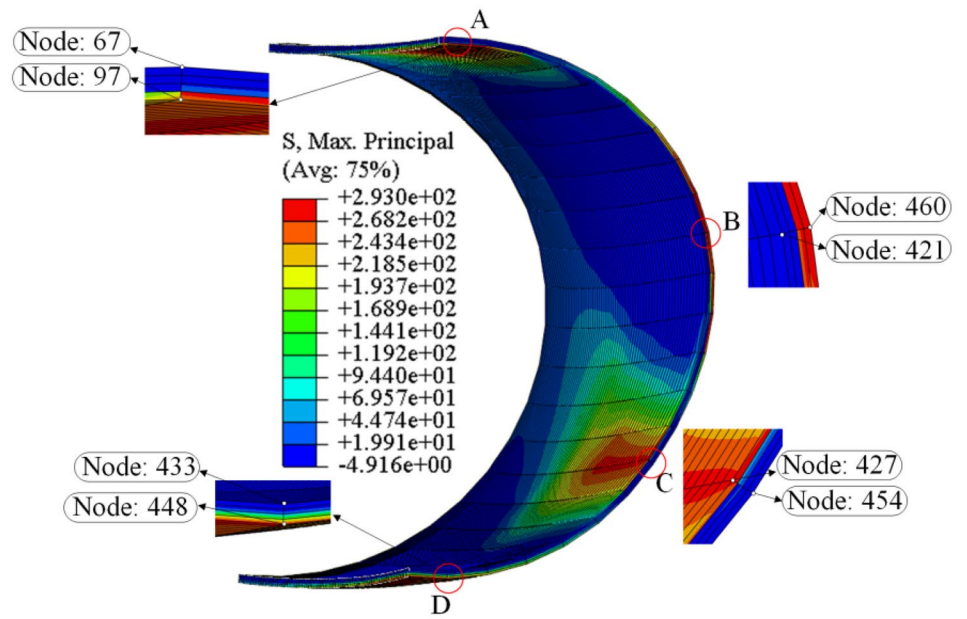
(a) Maximum principal stress

(b) Minimum principal stress

Table 3 Maximum and minimum principal stresses

Position	Node ID	Maximum principal stress (MPa)	Minimum principal stress (MPa)
A	67	—	−257
	97	+251	—
B	460	+282	—
	421	—	−281
C	454	—	−286
	427	+285	—
D	448	+277	—
	433	—	−269
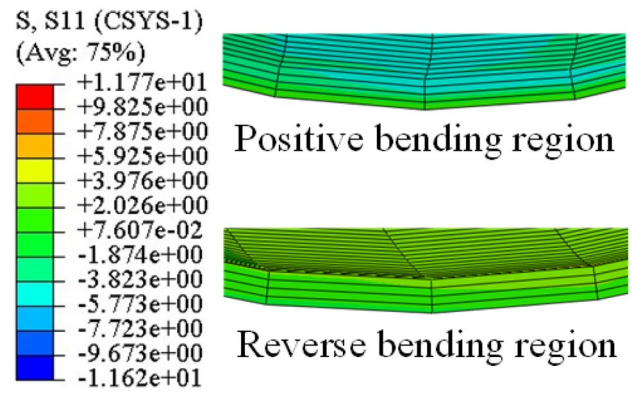
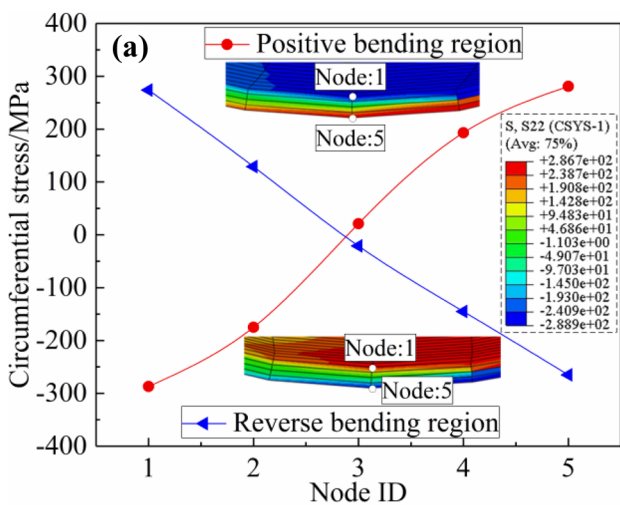**Fig. 13** Distribution of radial stress
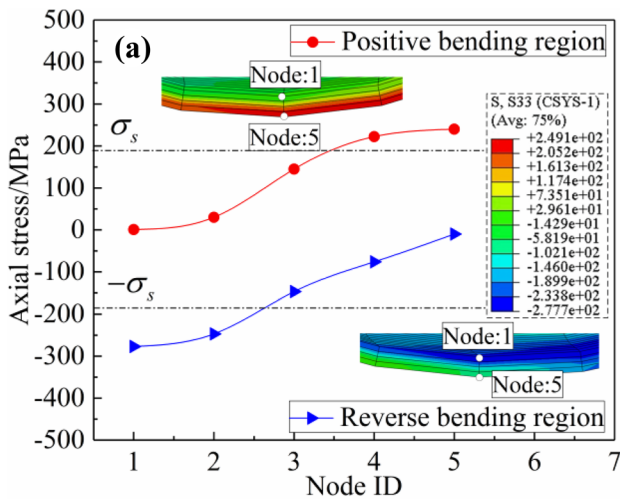
(a) Along the thickness direction
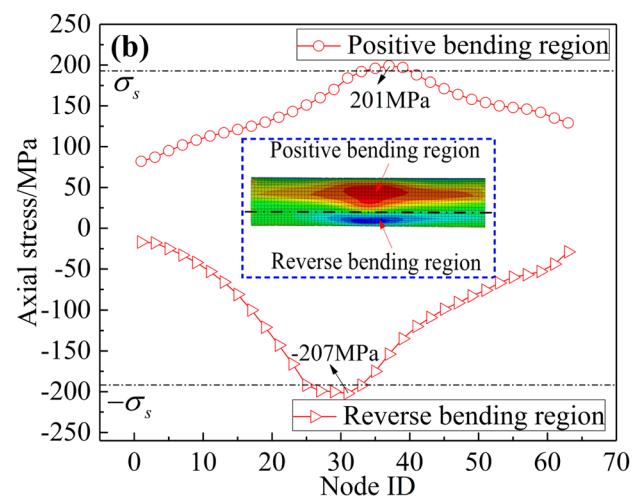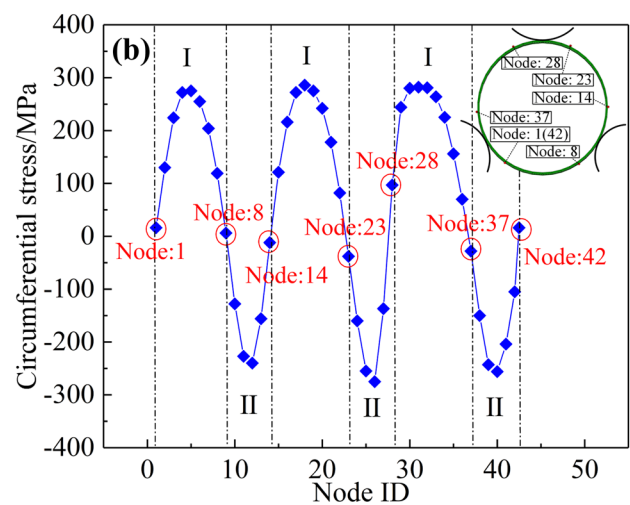

(b) Along the length direction

Fig. 11 Distribution of axial stress

(a) Along the thickness direction

(b) Along the circumferential direction

Fig. 12 Distribution of tangential stress (I: positive bending region; II: reverse bending region)
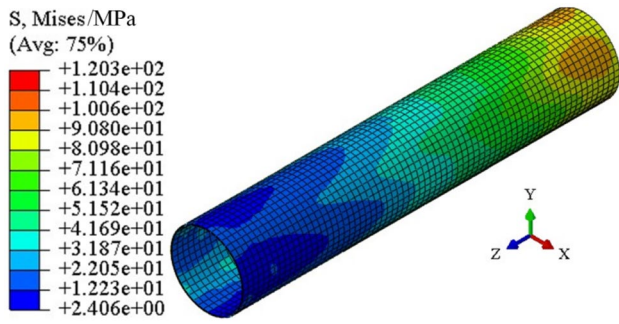
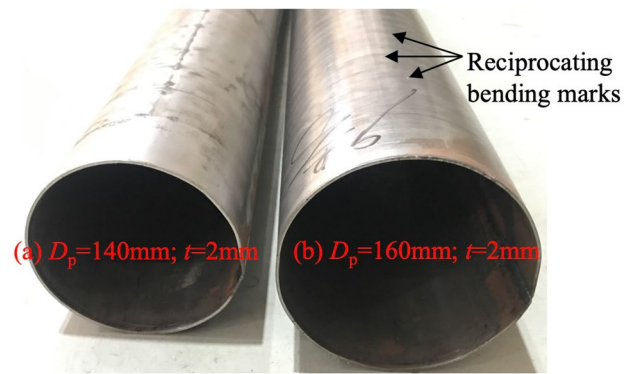**Fig. 14** Distribution of equivalent stress after calibration

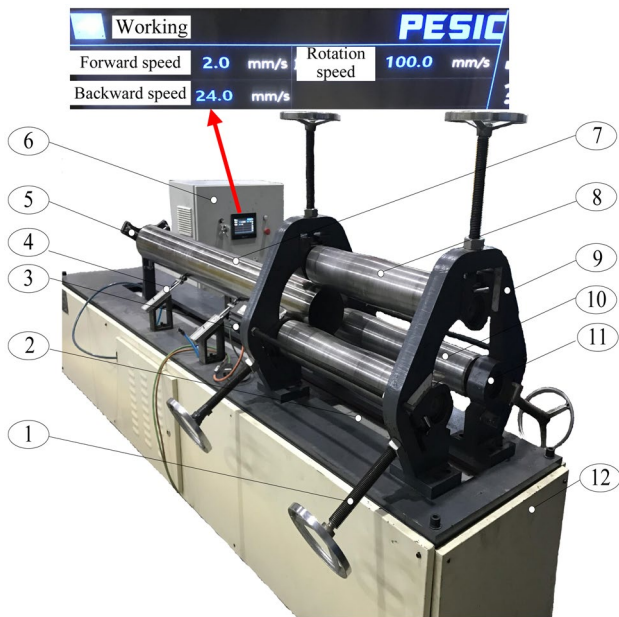**Fig. 16** Forming effect of ST12 pipes

Fig. 15 Experimental device for pipe calibration

As shown in Fig. 15, the roller is connected with the slider fixed on the frame via bearing. The slider can slide vertically along the frame surface via a screw to adjust the radial reduction of the three rollers. The support assembly keeps the balance of the pipe during the experiment. The servo motor drives two lower rollers to rotate synchronously, which drives the pipe and the upper roller to start turning. At the same time, the push plate drives the pipe to move along the slideway. So far, the calibration process of simultaneous rotation and movement of the pipe is realized. The pipes and rollers selected for the experiment are the same as the pipes and rollers selected for the simulation.

The experimental results of ST12 pipes after calibration are shown in Table 4. From Table 4, it can be observed that the residual roundness is within 0.7% and the residual straightness is within 0.2%. Both meet industry standard requirements [4]. The experimental results further verify that the calibration process of pipes is achieved by axial and circumferential reciprocating bending. The forming effect of ST12 pipes is shown in Fig. 16.

Table 4 Experimental results after calibration

Material	Length L_p (mm)	Initial roundness	Initial straightness	Outer diameter D_p (mm)	Thickness t (mm)	Residual roundness (%)	Residual Straightness (%)
ST12	1000	5%	10‰	140	2	0.58	0.15
					1.5	0.65	0.18
				160	2	0.64	0.17
					1.5	0.59	0.19

7 Conclusions

1. Theoretically, the reciprocating bending springback analysis of axial straightening and circumferential rounding are established, respectively. The deformation mechanism of the process is revealed. It is proved that the reciprocating bending can eliminate the difference of initial curvature, and unify the axial and circumferential curvature to the same direction and value. It provides theoretical support for the calibration process to be applied to actual production.

2. When the loading curvature tends to zero, the axial curvature after reciprocating bending is also close to zero. The straightness can be calibrated. When the loading curvature tends to a certain value, the circumferential curvature after reciprocating bending tends to be consistent. The roundness can be calibrated. The combination of axial reciprocating bending and circumferential reciprocating bending enables the calibration process of LSAW pipes.

3. The simulation results show that the distribution of the maximum and minimum principal stress accord with the characteristics of pure bending deformation; After unloading and springback, the residual stress is small and evenly distributed; the calibration process is mainly influenced by the synergy of axial stress and circumferential stress, which further supports the theoretical analysis results.

Authors contributions **Xueying Huang** was involved in the conceptualization, methodology, validation, formal analysis, investigation, data curation, writing—original draft, writing—review and editing, software and visualization. **Gaochao Yu** contributed to the conceptualization, methodology, formal analysis, supervision and writing—review and editing. **Chunge Wang** helped in the conceptualization, methodology, formal analysis and supervision. **Jun Zhao** contributed to the conceptualization, methodology, formal analysis and supervision.

Declarations

Ethical approval The authors declare that this manuscript was not submitted to more than one journal for simultaneous consideration. Also, the submitted work is original and not have been published elsewhere in any form or language.

Consent to participate and publish The authors declare that they participated in this paper willingly and the authors declare to consent to the publication of this paper.

Conflict of interest We declare that we have no financial and personal relationships with other people or organizations that can inappropriately influence our work, there is no professional or other personal interest of any nature or kind in any product, service and/or company that could be construed as influencing the position presented in, or the review of, the manuscript entitled, "*Deformation mechanism analysis of three-roller continuous and synchronous calibration process of straightness and roundness for LSAW pipes.*" The authors declare that there is no conflict of interests regarding the publication of this paper.

References

1. Deng D, Murakawa H, Liang W (2008) Numerical and experimental investigations on welding residual stress in multi-pass butt-welded austenitic stainless-steel pipe. Comput Mater Sci 42(2):234–244. https://doi.org/10.1016/j.commatsci.2007.07.009

2. Law M, Prask H, Luzin V, Gnaeupel-Herold T (2006) Residual stress measurements in coil linepipe and girth welded pipe. Mater Sci Eng, A 437(1):60–63. https://doi.org/10.1016/j.msea.2006.04.062

3. Yaghi A, Hyde TH, Becker AA, Sun W, Williams JA (2008) Residual stress simulation in thin and thick-walled stainless steel pipe welds including pipe diameter effects. Int J Press Vessels Pip 83(11–12):864–874. https://doi.org/10.1016/j.ijpvp.2006.08.014

4. ANSI/API Specification 5L (2012) Specification for line pipe (forty-fifth edition). Washington DC, United States

5. Yin J, Zhao J, Qu XY, Zhai RX (2011) Springback analysis of expanding and setting round for large diameter pipe. J Mech Eng 47(12):32–42. https://doi.org/10.3901/JME.2011.12.032

6. Yin J, Zhao J, Sun HL, Zhan PP (2011) Precise compression and setting round by mould for large pipes. Opt Precis Eng 19(9):2072–2078. https://doi.org/10.3788/OPE.20111909.2072

7. Zhao J, Zhan PP, Ma R, Zhai RX (2012) Control strategy of overbending setting round for pipe-end of large pipes by mould press type method. Trans Nonferrous Metals Soc China 22(S2):329–334. https://doi.org/10.1016/S1003-6326(12)61727-0

8. Zhao J, Zhan PP, Ma R, Zhai RX (2013) Quantitative prediction of reduction in large pipe setting round process. Chin J Mech Eng (Eng Ed) 26(4):722–729

9. Zhao J, Zhan PP, Ma R, Zhai RX (2014) Prediction and control of springback in setting round process for pipe-end of large pipe. Int J Press Vessels Pip 116(1):56–64. https://doi.org/10.1016/j.ijpvp.2014.01.006

10. Zhao J, Yu GC, Ma R (2016) A mechanical model of symmetrical three-roller setting round process: The static bending stage. J Mater Process Technol 231:501–512. https://doi.org/10.1016/j.jmatprotec.2016.01.002

11. Yu GC, Zhao J, Xing JJ, Zhao FP, Li SL (2017) Research on the symmetrical three-roller setting round process. J Mech Eng 53(14):136–143. https://doi.org/10.3901/JME.2017.14.136

12. Zhao J, Song XK (2014) Control strategy of multi-point bending one-off straightening process for LSAW pipes. Int J Adv Manuf Technol 72(9–12):1615–1624. https://doi.org/10.1007/s00170-014-5776-9

13. Zhao J, Song XK, Cao HQ, Liu J (2014) Press straightening control strategy of multi-step three-point bending for LSAW pipes. J Harbin Inst Technol 46(1):90–96. https://doi.org/10.11918/j.issn.0367-6234.2014.01.016

14. Zhao J, Song XK, Cao HQ, Liu J (2014) Principle of multi-point bending one-off straightening process for longitudinally submerged arc welding pipes. J Mech Eng 50(2):92–97. https://doi.org/10.3901/JME.2014.02.092

15. Yu GC, Zhai RX, Zhao J, Ma R (2018) Theoretical analysis and numerical simulation on the process mechanism of two-roller straightening. Int J Adv Manuf Technol 94(9):4011–4021. https://doi.org/10.1007/s00170-017-1120-5

16. Liu ZJ, Ma LD, Li JH, Du YK, Meng ZJ (2020) Accuracy analysis of six skewed-roll straightening process of tube. J Iron Steel Res 32(9):55–61. https://doi.org/10.13228/j.boyuan.issn1001-0963.20200014

17. Wang CG, Yu GC, Wang W, Zhao J (2018) Deflection detection and curve fitting in three-roll continuous straightening process for LSAW pipes. J Mater Process Technol 255:150–160. https://doi.org/10.1016/j.jmatprotec.2017.11.060

18. Wang CG, Zhang ZY, Zhai RX, Yu GC, Zhao J (2018) Cross-sectional distortion of LSAW pipes in over-bend straightening process. Thin-Walled Struct 129(AUG.):85–93. https://doi.org/10.1016/j.tws.2018.03.016

19. Cui F, Yang HL (2015) New understanding in the field of straightening theory. Heavy Mach 2–5. https://doi.org/10.3969/j.issn.1001-196X.2015.01.001

20. Huang XY, Yu GC, Zhai RX, Ma R, Zhou C, Gao CL, Zhao J (2021) Roller design and numerical simulation of three-roller continuous and synchronous adjusting straightness and roundness process on LSAW pipes. J Mech Eng 57(10):148–159. https://doi.org/10.3901/JME.2021.10.148

21. Huang XY, Yu GC, Zhao J, Mu ZK, Zhang ZY, Ma R (2020) Numerical simulation and experimental investigations on a three-roller setting round process for thin-walled pipes. Int J Adv Manuf Technol 107:355–369. https://doi.org/10.1007/s00170-020-05087-2

22. Huang XY, Zhao J, Yu GC, Meng QD, Zhai RX (2021) Three-roller continuous setting round process for longitudinally submerged arc welding pipes. Trans Nonferrous Metals Soc China 31(5):1411–1426. https://doi.org/10.1016/S1003-6326(21)65586-3

23. Zhao J, Yu GC, WANG HR (2017) A roller-type continuous and synchronous calibrating straightness and roundness equipment and processing method for pipes. Hebei: CN106623507A

24. Zhao J, Cao HQ, Zhan PP, Ma R (2012) Pure bending equivalent principle for over-bend straightening and its experimental verification. J Mech Eng 48(8):28–33. https://doi.org/10.3901/JME.2012.08.028

25. Zhao J, Yin J, Ma R, Ma LX (2011) Springback equation of small curvature plane bending. Sci China Technol Sci 54:2386–2396. https://doi.org/10.1007/s11431-011-4447-4